Title

Development of 18F-labelled Tris(2-pyridylmethyl)amine-based Chelator to Image Zinc Distribution in Prostate Cancer Models Using Positron Emission Tomography

Author

Ali, Umama

Publication Date

2021

Peer reviewed|Thesis/dissertation

Development of 18F-labelled Tris(2-pyridylmethyl)amine-based Chelator to Image Zinc Distribution in Prostate Cancer Models Using Positron Emission Tomography

by

Umama Ali

THESIS

Submitted in partial satisfaction of the requirements for degree of

MASTER OF SCIENCE

in

Biomedical Imaging

in the

GRADUATE DIVISION

of the

UNIVERSITY OF CALIFORNIA, SAN FRANCISCO

Approved:

DocuSigned by:
Robert Flavell
DE54D221721B45E...

Robert Flavell

Chair

DocuSigned by:
Youngho Seo
[illegible]

Youngho Seo

DocuSigned by:
Ella Jones
[illegible]

Ella Jones

DocuSigned by:
John Kurhanewicz
593BD10CA23A498...

John Kurhanewicz

Committee Members

Acknowledgements

I dedicate this thesis to my family, friends and colleagues who have helped me during this thesis project.

I would like to thank my principal investigator Prof. Robert Flavell for offering me the opportunity to work on this fascinating project and providing valuable supervision and great supports to allow me to contribute to the scientific community. I would like to thank the postdoctoral scholars in Flavell's group including Dr. Changhua Mu for his supervision and expertise on synthetic chemistry and radiochemistry, and the advice and assistance from Dr. Sinan Wang for the radiochemistry, Dr. Niranjan Meher and Dr. Anil Bidkar for the *in vitro* and *in vivo* assays. I would like to thank my committee members, Prof. Youngho Seo, Prof. Ella Jones, and Prof. John Kurhanewicz for their support and advice throughout the process. I am appreciative of working alongside great individuals at UCSF, gaining valuable knowledge, experiences and skills from the MSBI program, and participating in this research project. I would like to thank the funding support that this project had received.

I would like to thank my parents who have supported me endlessly throughout this experience. Thank you to my friends who have motivated me. Finally, thank you to the 2021 MSBI Class for making this a great school year.

Development of 18F-labelled Tris(2-pyridylmethyl)amine-based Chelator to Image Zinc Distribution in Prostate Cancer Models Using Positron Emission Tomography

Umama Ali

Abstract

While methods for early detection and risk stratification of prostate cancer (PCa) have greatly improved in recent years, there remains an unmet clinical need for improved methods to accurately detect and grade PCa non-invasively using imaging techniques. Zinc (Zn) has been studied as a target biomarker due to its unique physiology in the prostate. It accumulates in a healthy prostate to a remarkable high concentration, while it significantly decreases by 60-80% in de-differentiated PCa. Previous studies have examined this property as a potential biomarker for using imaging modalities such as MRI and fluorescence to characterize PCa, however, these techniques are not amenable to clinical translation. PET imaging has yet to be explored in detecting Zn for a tool of PCa diagnosis. This study focused on developing a novel probe, ^{18}F-labelled Tris(2-pyridylmethyl)amine-based (^{18}F-TPA), which exhibits excellent zinc specificity and targetability, cell membrane permeability, and low cytotoxicity. Once the cells uptake the radionuclides, they bind with intracellular free zinc ion and will not flux out of the cells. Thus, the ^{18}F-TPA PET imaging method could directly image zinc biodistribution and therefore be applied to detect alterations in zinc homeostasis in PCa and other diseases. **Methods**: This project started from the chemical synthesis of a precursor compound NO_2-TPA and a non-radioactive reference compound, ^{19}F-TPA for the subsequent synthesis and characterization of radioactive ^{18}F-TPA. ^{18}F-TPA was synthesized in a hot cell with NO_2-TPA reacting ^{18}F in the presence of kryptofix 222 and purified using semi-prep HPLC with the conditions determined by the co-injection of NO_2-TPA and ^{19}F-TPA. The quality of ^{18}F-TPA was ensured by co-injection with ^{19}F-TPA to an analytical HPLC showing the same retention time. Furthermore, ^{19}F-TPA was used to characterize Zn binding by determining a Zn^{19}F-TPA complex formation on an analytical HPLC. Subsequently the developed probe was used to test the hypothesis of its trapping behavior when bound to Zn^{+2} using an in vitro cell binding assay. One group had only the probe while two other groups had TPEN, a known strong Zn chelator, and TPA that were used as blocking agents followed by the introduction of the probe. The radioactivity was measured using a Hidex gamma counter with results recording in counts per minute. **Results**: The ^{18}F-TPA probe was successfully developed and purified with high yield. The cell binding assay provided evidence of the

possibility the probe can be internalized when it binds to intracellular Zn^{+2}. This was evidenced by high counts per minute (CPM) levels in cells with only probe uptake. In comparison, the cells with TPEN and TPA as blocking agents demonstrated low CPM levels. This provides preliminary evidence that the probe is Zn^{+2} specific. However, further in vitro assays need to be conducted with consideration of separating the membrane from the internal components of the cell. Without this consideration, it can be concluded that the probe is membrane-bound and not essentially trapped in the intracellular space of the cell. **Conclusion**: A new Zn^{+2} binding PET imaging radionuclide was developed and utilized for subsequent *in vitro* and *in vivo* assays. The *in vitro* cell binding assays have provided promising results that may support the hypothesis of cell internalization of the probe as it binds to Zn. The work on the in vitro assays and animal studies are still in progress. Future work will focus on additional *in vitro* assays and performing *in vivo* assays. The results from this study thus far have been encouraging on the potential of this probe as a diagnostic tool to examine zinc distribution.

Table of Contents

List of Figures

List of Abbreviations:

^{18}F-TPA - ^{18}F-labelled Tris(2-pyridylmethyl)amine

^{19}F-TPA - ^{19}F-labelled Tris(2-pyridylmethyl)amine

CPM - Counts per minute

PCa - Prostate Cancer

PET - Positron Emission Tomography

PSA - Prostate-specific antigen

TPA - Tris(2-pyridylmethyl)amine

TPEN - N,N,N′,N′-tetrakis(2-pyridinylmethyl)-1,2-ethanediamine

Zn - Zinc

Zn^{+2} - Zinc ions

Introduction

According to the statistics released by the US Centers for Disease Control and Prevention in 2017, prostate cancer (PCa) is rated as the most prevalent disease occurring almost twice as much as lung and bronchus cancers, and the second leading cause of cancer deaths in the US.[1] Its high morbidity is a result from the lack of symptoms and robust screening methods during the early stages.[2]

Current methods of PCa detection rely on clinical history, biopsy grade, serum prostate-specific antigen (PSA) levels, physical examination, and presence of gross local invasion or metastasis, which are inaccurate, invasive, and prone to errors due to patient differences. PSA, a common biomarker used to screen PCa, exhibits false positive rates as high as 75%. Only about 25% of men with elevated PSA resulted in biopsy confirmation of PCa.[2,3] Advanced modern non-invasive imaging technologies, such as CT, X-ray, and optical imaging have been used for early diagnosis however they can only image tumor changes at the anatomic level because of their limited sensitivity and specificity. Another modality, MRI, has become an important tool for the diagnosis of PCa and is widely used today. However, MRI has similar challenges to other modalities and has other challenges that limits its application. About 5-20% of lesions detected by MRI scans are considered clinically significant cancers either invisible or greatly underestimated and false negative rates are as high as 30%.[4] MRI also has a lot of false positive as it relates to comorbidities the patient may have such as infection, inflammation, and hyperplasia.[4] With these current challenges, there is a clinical need for a sensitive and accurate method for the diagnosis of aggressive PCa.

To meet this need for accurate detection of PCa, there has been exploration in identifying biomarkers. Zinc (Zn) has been identified as a potential biomarker due to its unique physiology in the prostate. Zn is a ubiquitous mineral that is fundamental for many cellular processes such as DNA replication and metabolic activity.[5] Zn transporters maintains the tightly regulated cellular and subcellular localization.[6,7] In many cell types, Zn(II) is stored in secretory vesicles, released upon stimulation, and packed in secretory granules with insulin resulting in a high zinc concentration of 20-500 mM.[7,8]

As a key regulatory factor in the intermediary metabolism of prostate cells, Zn is essential. The prostate gland's role is producing and secreting prostatic fluid that becomes an essential component for seminal fluid.[10]

It contains high levels of citrate (30-80-fold) and Zn (10-20 fold) than in other soft tissues.[10] In normal prostate, Zn enters the cell through ZIP transporters and leaves via ZnT-1 transporters. Mitochondrial (m-) aconitase, an enzyme that catalyzes the first step in the Krebs cycle, is inhibited by Zn thus preventing the oxidation of citrate to isocitrate (Figure 1).[10] Citrate is then exported to the cytosol and secreted into the acini lumen accumulating in high levels during prostatic fluid production.[11] This metabolic pathway is unique to the prostate, known as net citrate production.[11] The inhibitory effect by Zn is more efficient in prostate cells than in non-prostate cells under aerobic conditions. In non-prostate cells, Zn levels are not sufficiently high to inhibit m-aconitase.[10] The high accumulation of Zn additionally inhibits proliferation and induces apoptosis in the prostate.[10] As Zn crosses the outer mitochondrial membrane, it induces Bax to form pores that allow cytochrome c to be released and interact with caspases to cause apoptosis (Figure 1).[10] This apoptotic function is essential in managing the growth of the cell.

As PCa develops, Zn and citrate levels are reduced. The expression of both Zn transporters that allow Zn to enter and leave the prostate cell are expressed at low levels.[10] This in turn decreases the Zn levels in the cell resulting in its loss of inhibitory effect on m-aconitase.[10] Allowing for citrate to oxidize and yield higher ATP levels.[10] When the cells become malignant, the increase in energy production promotes proliferation and diminishes the pro-apoptotic effect that Zn normally induced.[10]

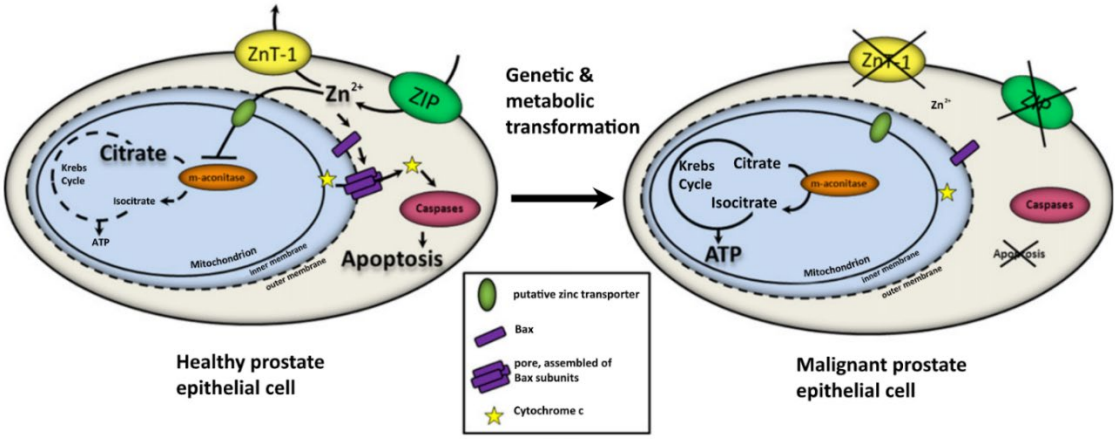

Figure 1: Biological process of Zn^{2+} and citrate in healthy prostate cell (left image) and in malignant prostate cell (right image). In the healthy prostate cell, Zn^{2+} presents in high levels and acts as an inhibitor in the Krebs cycle which increases in citrate levels and promotes apoptosis. In the malignant prostate cell, due to low Zn^{2} concentrations, its inhibitory and pro-apoptotic effects are abolished.[10]

There is overwhelming data that establishes Zn is always decreased in PCa.[11] Zn accumulates to high concentrations in health prostate while it is significantly decreased by 60-80% in PCa.[12] Normally, prostate cells have an upregulation of ZIP1 zinc specific transporter that allows for intracellular accumulation of Zn resulting in a complex formation with citrate and secretion into prostatic fluid.[12] Consequently, this property of Zn accumulation is lost. Therefore, this progressive loss of Zn is representative of an excellent biomarker for PCa progression.[13] Furthermore, it is well established through *in situ* Zn staining of prostate tissues the decrease in tissue Zn concentrations is due to the decrease in malignant cells compared to high Zn concentrations in healthy prostate cells.[11] PCa is the only known prostatic disease associated with decreased levels of Zn as other prostatic diseases such as prostatitis and benign prostatic hyperplasia (BPH) do not exhibit this phenomenon.[13] Thus, Zn makes an excellent biomarker for early detection of PCa which can be utilized by an imaging agent sensitive to Zn concentrations.[13]

The first report of Zn as a biomarker for early PCa detection was done using a fluorescent sensor by Ghosh et al.[13] The study employed a novel Zn fluorescent sensor ZPP1 to monitor the transformation of malignant cells in a transgenic adenocarcinoma of the mouse prostate (TRAMP) model. This sensor precisely bound two Zn ions and could observe tumor progression in an age-dependent manner as it related to decreases in fluorescence intensity.[13] The study was successful in developing a sensor that had high sensitivity and specificity, high accuracy, high Zn selectivity, and easy to use to detect and quantify Zn for PCa detection.[14] However, optical imaging itself is difficult to translate into clinical practice due to limitations of light penetration with whole-body deep tissue; in doing so it would require invasive endoscopic imaging.[2]

MRI was explored as an alternative to optical imaging a few years later. One study used a Zn binding gadolinium agent to detect extracellular Zn and glucose-stimulated Zn secretion using proton MRI.[15] Jordan et al. were able to distinguish healthy versus malignant mouse prostates as early as 11 weeks of age. [15] With a combination of different invasive measurements, with histological confirmation, small malignant lesions could be identified providing an option for targeted biopsy. [15] With the use of MRI, the study confirmed a loss of Zn secretion in prostate malignant lesions. [15] The study demonstrated the use of glucose-stimulated Zn(II) release from prostate cells as a new specific diagnostic method.

Recently, another MRI study was done using ^{19}F ion chemical exchange saturation transfer (iCEST) and 5,5',6,6'-tetrafluoro 1,2-bis(o-aminophenoxy)ethane-N,N,N',N'- tetraacetic acid (TF-BAPTA) as a fluorinated zinc probe. [2] Yuan et al. presented an alternative method to detect Zn in vivo that used a combination of ^{19}F MRI and chemical exchange saturation transfer (CEST) to monitor Zn ion (Zn^{2+}) with TF-BAPTA specifically.[2] TF-BAPTA had limited cell permeability and thus could only bind to extracellular Zn. The study was able to discriminate normal and malignant prostate cells with a 10-fold higher sensitivity than the method presented by Jordan et al.[2] Since ^{19}F MRI and iCEST are clinically available, this method has high translational potential for PCa diagnosis. However, despite these advantages from these MRI studies, further exploration is needed to develop Zn detection strategies that have high specificity and sensitivity for aggressive PCa diagnosis.
This thesis aims at meeting these urgent clinical needs in developing a new and reliable positron emission tomography (PET) imaging method to provide precise treatment guidance to patients with PCa. The focus will be on developing ^{18}F labelled radionuclide to image the homeostasis of intracellular Zn^{2+} in prostate for the cancer detection.

No current studies have explored utilizing PET to image zinc distribution as a tool for PCa diagnosis. In the context of molecular imaging, PET is a powerful imaging modality with greater sensitivity than MRI.[16] Its ability to detect and quantity a radiolabeled tracer, PET is a versatile and dominant imaging modality for the diagnosis and characterization of the molecular biology of a disease. [16] Due to the low concentrations of the radiolabeled tracers needed, most notable fludeoxyglucose (FDG) as a dominant diagnostic agent, PET is significant in establishing hallmarks of malignancy including increased proliferation. [16]

The feasibility of Zn imaging with PET has been demonstrated in prior studies. Vasdey et al. developed copper (Cu)/Zn chelators as a PET imaging agent for metal-rich Alzheimer's disease (AD).[17] Cary et al. developed functional ligands with a tight Cu binding affinity and demonstrated binding to antibody and AD-affected brain slices.[18] These prior studies demonstrate the feasibility of imaging endogenous trace metals pools such as Cu or Zn for the detection of cancer.

Accordingly, the proposal aims to design an imaging method to image the homeostasis of Zn in prostate using PET. This will be done by developing an ^{18}F isotope-labeled PET imaging radionuclide with a specific

zinc chelating scaffold tris(2-pyridylmethyl)amine (TPA). TPA is a commonly used tripodal ligand scaffold for the coordination chemistry of transition metals. [19] The TPA compound (Figure 2A) has nitrogen-based donor groups that allow the compound to selectively bind to borderline transition metals. [19] The affinities for the first row of transition metal ions follows the Irving-Williams series. [19] With regards to zinc, it has the coordination of a 1:1 stoichiometry and 10 pM affinity. [19] The tertiary amine has a pKa 6.17 therefore at physiological pH, a small fraction of the chelator is protonated. [19] TPA has been found to have excellent zinc specificity and targetability, cell membrane permeability, excellent water solubility, small in size, and low cytotoxicity. [19]

The ^{18}F-TPA radiolabeled probe is expected to be taken up by the cell, bind with intracellular free zinc to form a positively charged complex, and will be retained within the cell.[19] Figure 2B depicts this cell permeable zinc chelator based on a TPA scaffold. As the radionuclide decays, it will emit positrons and the resulting gamma rays that can be detected by the PET scanner. This cell trapping property of TPA can be leveraged to generate image contrast.

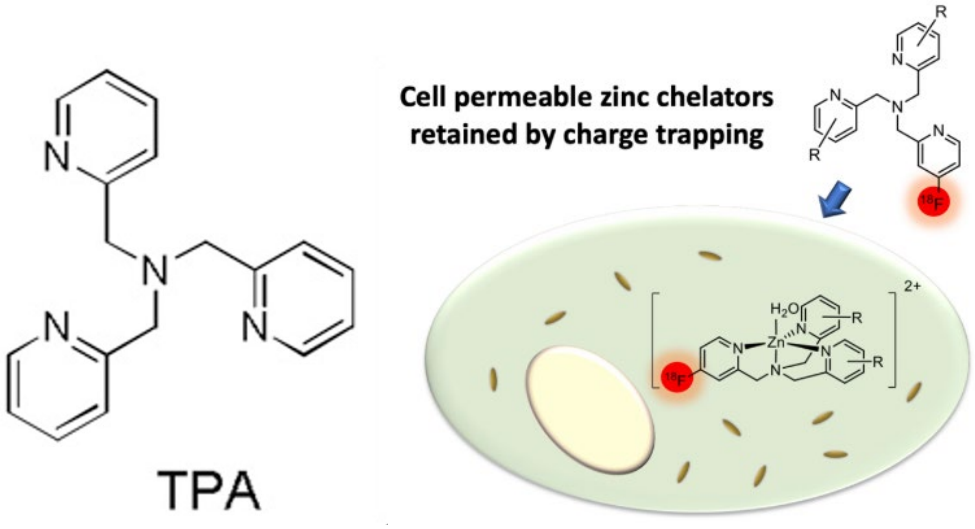

Figure 2. Left image (2A) and right image (2B). **2A:** The chemical structure of TPA.[19] **2B:** PET zinc tracer design. Cell permeable zinc chelator based on the tripicolylamine scaffold that is administered, binds to intracellular Zn, acquires a positive charge, and is retained in the cell.

This ^{18}F-TPA zinc sensing probe was characterized and evaluated in *in vitro* assays followed by *in vivo* PET imaging study with a wild type of male mice. Once synthesis was complete, the probe was used to validate its effectiveness in detecting zinc as demonstrated with the *in vitro* assays. Zn poor and prostate cancer cell

lines were used to validate ^{18}F-TPA binding with specificity demonstrated by utilizing cell binding assays using zinc chelators. With the success of the *in vitro* studies, *in vivo* assays were performed using ^{18}F-TPA probes to detect zinc in well characterized PCa mouse model. Whole body distribution studies of ^{18}F-TPA probe in wild type male mice were performed from PET imaging results. This study has set the stage for future applications of ^{18}F-TPA as a probe in disease settings for other diseases.

The ^{18}F-TPA probe developed and successfully utilized to detect zinc distribution has provided encouraging results. This study has the potential to be further extended of ^{18}F-TPA as a probe in other disease applications. The study has yielded a specific PET imaging mechanism to examine zinc distribution through demonstrating its feasibility *in vitro* and *in vivo* studies. Overall, this study has provided motivation to explore the feasibility of translating this PET imaging technology into human clinical applications with the goal of improving guidance for the treatment of PCa.

Methods

A. Radiosynthesis

Synthesis and characterization of ^{19}F-TPA

^{19}F- TPA was synthesized and developed as a reference compound to characterize ^{18}F-TPA according to the reported method with some modifications.[20] Di-(2-picolyl)amine (20 mg) , 2-(bromomethyl)-4-fluropyridine hydrobromide (25 mg) and K_2CO_3 (22 mg) were dissolved in 15mL of anhydrous CH_3CN. The mixture was stirred under N_2 atmosphere at room temperature for 24 hours followed by filtration and evaporation under a vacuum. Brine (15 mL) was added to the resulting residue and the organic layers was extracted by CH_2Cl_2 (3 × 15 mL). The organic layers were combined, dried over Na_2SO_4, filtered, and evaporated under a vacuum to dryness. The resulting residue was extracted and purified with pentane (3 ×15 mL) for 10 minutes. The organic layers were combined and evaporated under a vacuum to obtain the resulting product of ^{19}F-TPA. The ^{19}F-TPA compound was characterized using a 400 MHz ^{1}H Nuclear Magnetic Resonance (NMR) spectrometer with ^{1}H, ^{13}C, and ^{19}F NMR spectra acquisition to validate that the synthesis was successful. ^{1}H NMR spectrum of ^{19}F-TPA (400 MHz, CDCl3) had the following chemical shift: δ 8.57 (d, J = 4.50, 2H), 8.50 (dd, J = 8.6, 5.6 Hz, 1H), 7.69 (td, J = 7.7, 1.8 Hz, 2H), 7.56 (d, J = 7.8 Hz, 2H), 7.40 (dd, J = 9.9, 2.7 Hz, 1H), 7.18 (ddd, J = 7.5,

4.9, 1.3 Hz, 2H), 6.91 (ddd, J = 8.3, 5.6, 2.6 Hz, 1H), 3.91 (s, 6H). ^{13}C NMR spectrum of F-TPA (100 MHz, $CDCl_3$) had the following chemical shift: δ 170.61, 168.00, 163.38, 158.96, 151.38, 149.23, 136.53, 122.98, 122.16, 60.24, 59.77, 59.74. ^{19}F NMR spectrum of F-TPA (400 MHz, $CDCl_3$) had a chemical shift of δ -102.56.

^{19}F-TPA Zn binding study

The conversion of ^{19}F-TPA to its zinc bound form was tested using an analytical high performance liquid chromatography (HPLC) assay. A sample of ^{19}F-TPA was prepared in a microcentrifuge tube with ~400 µL of CH_3CN. The cold ^{19}F-TPA was tested first to determine its retention time. The Zn was prepared with $ZnSO_4$ dissolved in ~400 µL of H_2O in a new microcentrifuge tube. A solution of ^{19}F-TPA and Zn was prepared by taking 100 µL from each sample into a new microcentrifuge tube and tested using the analytical HPLC. Additional Zn solution was added to this mixture to increase Zn concentration and then tested with the HPLC. Overall, this yielded different retention times for the Zn^{19}F-TPA complex and ^{19}F-TPA compound as the concentration of Zn increased. A Luna 5 µm C18(2) reversed phase column was used with a mobile phase of CH_3CN: H_2O of 40:60 at a wavelength of 254 nm and flow rate of 1 mL/min.

Synthesis and characterization of NO_2-TPA

The precursor for ^{18}F-TPA, NO_2-TPA, was synthesized according to the reported method with some modifications.[20] The starting material, 2-(bromomethyl)-4-nitropyridine, was synthesized first. 4-(nitropyridine-2-yl)methanol (154.1 mg) was dissolved in 15 mL of CH_2Cl_2 then flushed with N_2 for 5 minutes. The solution was placed in an ice water bath followed by the addition of 2.2 mL of PBr_3 dropwise. The mixture was warmed to room temperature, stirred for 2 hours under N_2 atmosphere, then refluxed for 1 hour at 53°C under N_2 atmosphere. After the solution was cooled to room temperature, 10mL of H_2O was added and stirred, then 15 mL of K_2CO_3 (25 mg) aqueous solution was added. Brine (5 mL) was added, and the organic layer was extracted by CH_2Cl_2 (2 × 15 mL). The organic layers were combined, dried over Na_2SO_4, filtered, and evaporated under a vacuum to dryness. 2-(bromomethyl)-4-nitropyridine product was used immediately for the workup of NO_2-TPA due to its instability.

Di-(2-picolyl)amine (100 mg), 2-(bromomethyl)-4-nitropyridine hydrobromide and K_2CO_3(198.2 mg) were dissolved in 15 mL of anhydrous CH_3CN. The mixture was stirred under N_2 atmosphere at room

temperature for 24 hours followed by filtration through a fine filter paper to remove the suspension. The filtrate was collected and evaporated to dryness to obtain a brown residual. A TLC was done to verify the separation of the product by optimization of the mobile phase consisting of CH_2Cl_2 and methanol. The resulting product was purified by a column chromatography with silica gel and eluted by a mixture of CH_2Cl_2 and methanol with a ratio of 10:0.8.

Determination of semi-prep HPLC conditions

To order to isolate ^{18}F-TPA from unreacted starting material NO_2-TPA using semi-prepare HPLC, ^{18}F-TPA's model compound ^{19}F-TPA was mixed with NO_2-TPA in DMSO and co-injected into the HPLC. Optimization of HPLC condition was needed for a good separation of NO_2-TPA and ^{18}F-TPA as only a small portion of NO_2-TPA is converted to ^{18}F-TPA, which needs to be isolated from this precursor. A mixture of NO_2-TPA and ^{19}F-TPA was mixed and eluted with an analytical HPLC on an ultraviolent (UV) detector channel, at a wavelength of 254 nm, with a variety of combination ratio of a mixture of acetonitrile and water through a Luna 10 μm C18(2) reversed phase column at a fluid rate of 5 mL/min. The ^{19}F-TPA compound retention time was determined first before determining the separation conditions.

Radiosynthesis and characterization of ^{18}F-TPA

^{18}F-TPA probe was synthesized is depicted in Figure 3B according to the previously reported methods.[21] $K^{18}F$ solution obtained from the cyclotron (2 mL, ~40-50 mCi) was passed through a QMA scientific type cartridge to remove water and trap ^{18}F. The cartridge was activated prior to experimental use with a rinse of 4 mL of 1M Na_2CO_3 solution followed by 12 mL of H_2O. An elution mixture of Kryptofix 222 (11 mg), CH_3CN (800 μL), and $KHCO_3$ (100 μL) was passed through the cartridge into a vial followed by 6 mL of H_2O into a new vial. The solution was dried under vacuum and heated at 115°C with N_2 blowing into the vial for 6 minutes. Anhydrous CH_3CN (1 mL) was added to the solution, heated and evaporated under vacuum for 3 minutes, repeated twice. A mixture of NO_2-TPA (3 mg) dissolved in 1mL of anhydrous DMSO was added to the dried solution and heated to 150 °C for 15 minutes once to yield ^{18}F-TPA. The ^{18}F-TPA compound was purified from the reaction solution by a semiprep HPLC using above-found solvent condition (CH_3CN:H_2O = 40:60). ^{18}F-TPA was isolated from the solvent mixture (CH_3CN and H_2O mixture) by first diluting the sample

to decrease the amount of CH_3CN below to 10%. This diluted solution was then passed through a pre-conditioned HLB cartridge to remove water and trap ^{18}F-TPA. Afterwards, some air was blown into the cartridge using a syringe to remove as much water as possible. The cartridge was then rinsed with 5mL of ethanol and the elute, the ^{18}F-TPA, was collected. The eluent was dried under vacuum at 115 °C for 6 minutes to get the pure compound remaining and then reformulated in phosphate-buffered solution (PBS) for subsequent studies. The ^{18}F-TPA was characterized with the analytical HPLC to determine its retention time. Afterwards, ^{18}F-TPA was characterized with an analytical HPLC by mixing it with ^{19}F-TPA via comparison of the retention of ^{18}F-TPA and ^{19}F-TPA in UV and radiation (Rad) channels.

B. *In Vitro* Study

Uptake and Validation of ^{18}F-TPA zinc binding in *in vitro* assays

An uptake assay was conducted in zinc poor cell line HEK293-T and prostate cancer cell line 22Rv1.[22] The ^{18}F-TPA probe uptake was tested with a blocking experiment to validate the proof of cellular uptake. The cells were maintained in a humidified incubator under 5% CO_2 atmosphere at 37°C in RPMI-1640 media supplanted in 10% fetal bovine serum, 100 units of penicillin, and 100 ug/mL streptomycin. Around 1 million cells/well were seeded in 6-well plate 24 hours prior to the experiment.

The experiment was done in triplicate. The first group was the control and didn't contain the probe. The second group was used for the uptake assay in which only the ^{18}F-TPA probe was introduced. The third and fourth group were used for the cell binding assay using two blocking agents, N,N,N′,N-tetrakis(2-pyridylmethyl) ethylenediamine (TPEN) and ^{19}F-TPA, followed by the addition of ^{18}F-TPA probe. The cells were washed three time with PBS then placed in zinc free media, RPMI1640. An excess of 1μM of N,N,N′,N-tetrakis(2-pyridylmethyl) ethylenediamine (TPEN) was introduced into the third group of cells then incubated for 1hr. TPEN is an orthogonal, cell permeable zinc chelator, chemically distinct from TPA, that chelates free zinc.16. 1μM of ^{19}F-TPA was added into the fourth group of cells then incubated for 1 hour.

For each group followed by their respective incubation times, ~0.74 MBq-1.11 MBq (20-30 μCi) of ^{18}F-TPA was added containing 150 μL of PBS and then incubated for 2 hours. Then the cells were washed three times with PBS. The cells in each well were digested for 1h at room temperature in 1mL of a 1:1 mixture of

concentrated sulfuric and nitric acids.[18]After digestion, 5 % Triton X-100 solution (1.5mL) in water was added and transferred to vials where radioactivity was then measured using hidex gamma counter. The radioactivity was recorded in counts per minute (CPM). After measuring radioactivity, the vials were sonicated for 10 min to dissolve it completely.[18] The sample solution was transferred to a 15 mL centrifuge tube and diluted to 10 mL with inductively coupled plasma (ICP) matrix. It will then be processed for total Zn concentration analysis by inductively coupled plasma optical-emission spectrometry (ICP-OES) the core facility at University of California, Santa Cruz.[17,18]Statistical significance of differences of cell uptake amongst the groups will be compared via a one-way ANOVA with Holm-Sidak correction for multiple testing.

C. µPET/CT Imaging Study

Animal Model

The animal study was reviewed and approved by the University of California, San Francisco Institutional Animal Care and Use committee (UCSF-IACUC). The experiment was conducted on 3 wild type 5-week-old nude male mice and imaged at the imaging suite at the UCSF Department of Radiology and Biomedical Imaging at China Basin Campus.

Experimental Procedure

The biodistribution of ^{18}F-TPA in the mice was studied using PET imaging and biodistribution analysis. The uptake in the organs were compared with endogenous zinc concentration. The Siemens Inveon imaging system (Siemens, Munich, Germany) is comprised of two independent scanners, the Inveon dedicated PET and the Inveon CT scanner and both were used in this experiment.

The 3 mice were be anesthetized using isoflurane followed by intravenous tail injection of 100uL of ~3.7MBq-7.4MBq (100-200 uCi) ^{18}F-TPA in PBS and microPET/CT imaging. Immediately after injection, the mice were imaged for 1 hour using a dynamic scan protocol. The mice were then be imaged for a static scan, 2 hours post injection, for 20 minutes with 10 minutes for PET and 10 minutes for CT. Another static scan was obtained 4 hours post injection with 20 minutes for PET and 10 minutes for CT imaging. Since the signal may be weaker 4 hours post injection scan, the amount of time for the PET scan increased. The mice were anesthetized with isoflurane prior to scanning 2 hours and 4 hours post injection. PET imaging data was

acquired in list mode and reconstructed with the iterative OSEM 2-D reconstruction algorithm provided by the manufacturer.

Biodistribution Analysis

The mice were sacrificed after the completion of the scan and the radioactivity in the organs was measured using a hidex gamma counter. Blood was obtained by cardiac puncture. The liver, heart, brain, kidney, lung, spleen, stomach, small intestine, large intestine, pancreas, muscle, bone, and prostate were harvested.

After radioactivity decay, the samples were digested for 2 days at room temperature in 1mL of 1:1 mixture of concentrated sulfuric and nitric acids followed by addition of 1.5mL of 5% Trixton X-100 solution in water.[18] The samples were then sonicated for 90 minutes and 1mL of the sample solution was transferred to a 15mL centrifuge tube.[18] The solution was then diluted to 10mL with ICP matrix. The samples will be sent to the core facility at University of California, Santa Cruz ICP-OES analysis of total Zn concentration.[18] Uptake of ^{18}F-TPA in each organ will be reported as percent injected activity per gram of tissue. Total Zn concentration will be reported as nmol per gram of tissue.

Results

A. Radiosynthesis

Characterization of ^{19}F-TPA

Given the specific reaction conditions and safety issues of radioactive ^{18}F-TPA, its characterization and purification only relies on HPLC. Therefore, the cold ^{19}F-TPA compound was used as a reference compound to characterize and purify ^{18}F-TPA, synthesized based on the reaction schematic in **Figure 3A**. ^{19}F-TPA has been successfully synthesized as shown by the NMR spectra provided in Figures 4-6. It has been characterized by ^{1}H (Figure 4), ^{13}C (Figure 5), and ^{19}F NMR (Figure 6) showing successful synthesis with high levels of purity.

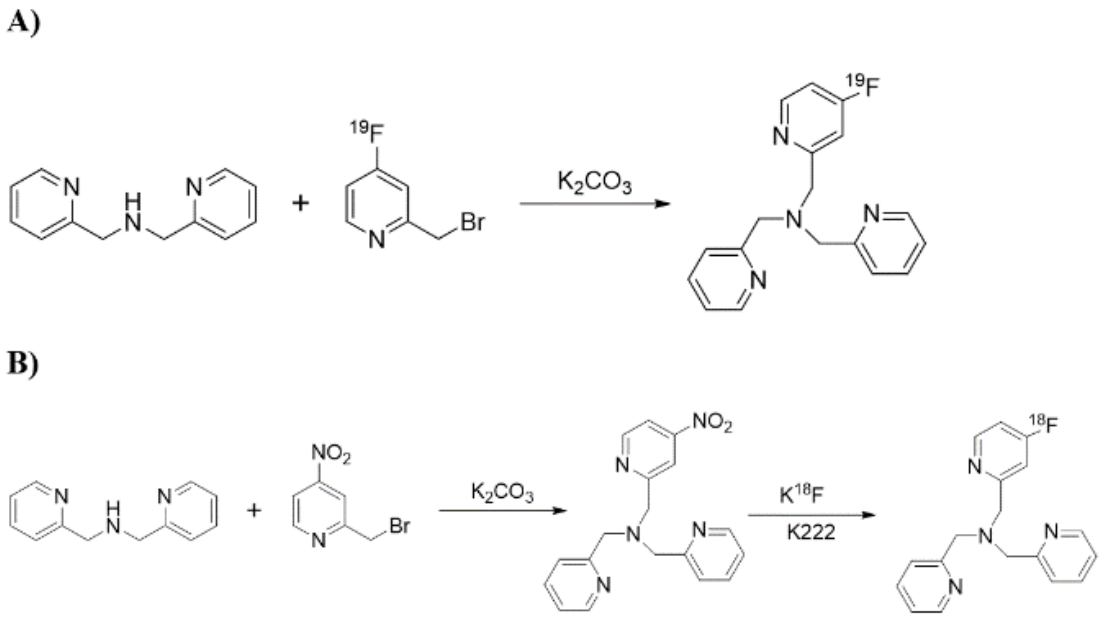

Figure 3. Synthetic and radiosynthetic scheme to obtain ^{19}F-TPA and ^{18}F-TPA. A) Synthesis of ^{19}F-TPA. B) Radiosynthesis of ^{18}F-TPA.

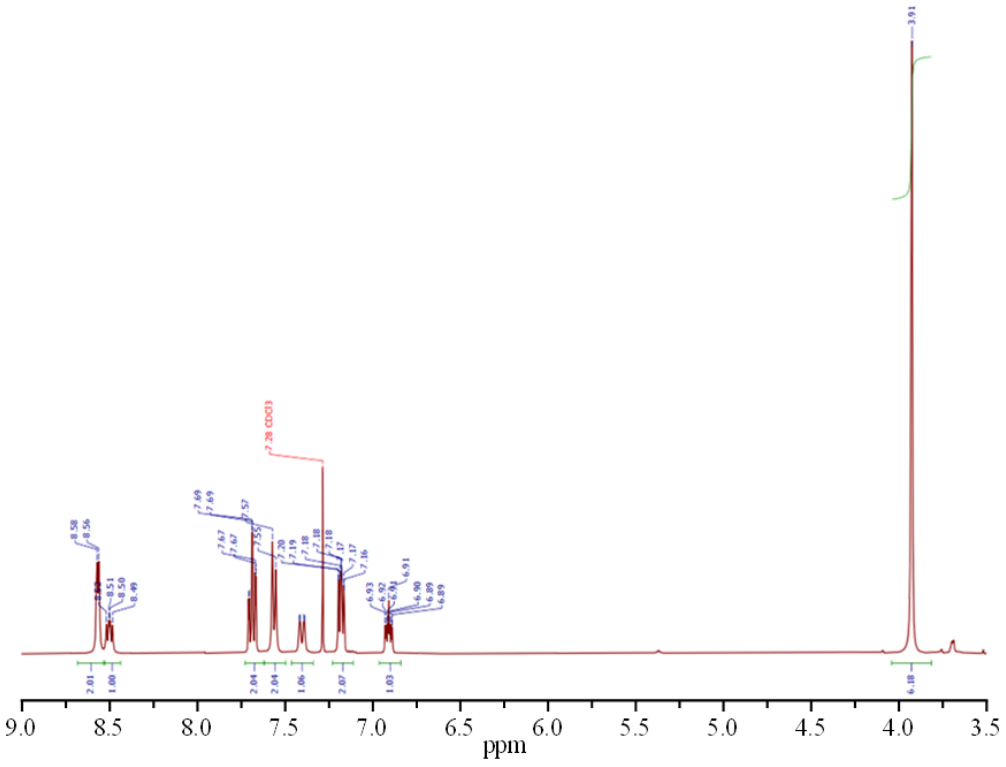

Figure 4. ^{1}H NMR spectrum of ^{19}F-TPA (400 MHz, $CDCl_3$). δ 8.57 (d, J = 4.50, 2H), 8.50 (dd, J = 8.6, 5.6 Hz, 1H), 7.69 (td, J = 7.7, 1.8 Hz, 2H), 7.56 (d, J = 7.8 Hz, 2H), 7.40 (dd, J = 9.9, 2.7 Hz, 1H), 7.18 (ddd, J = 7.5, 4.9, 1.3 Hz, 2H), 6.91 (ddd, J = 8.3, 5.6, 2.6 Hz, 1H), 3.91 (s, 6H).

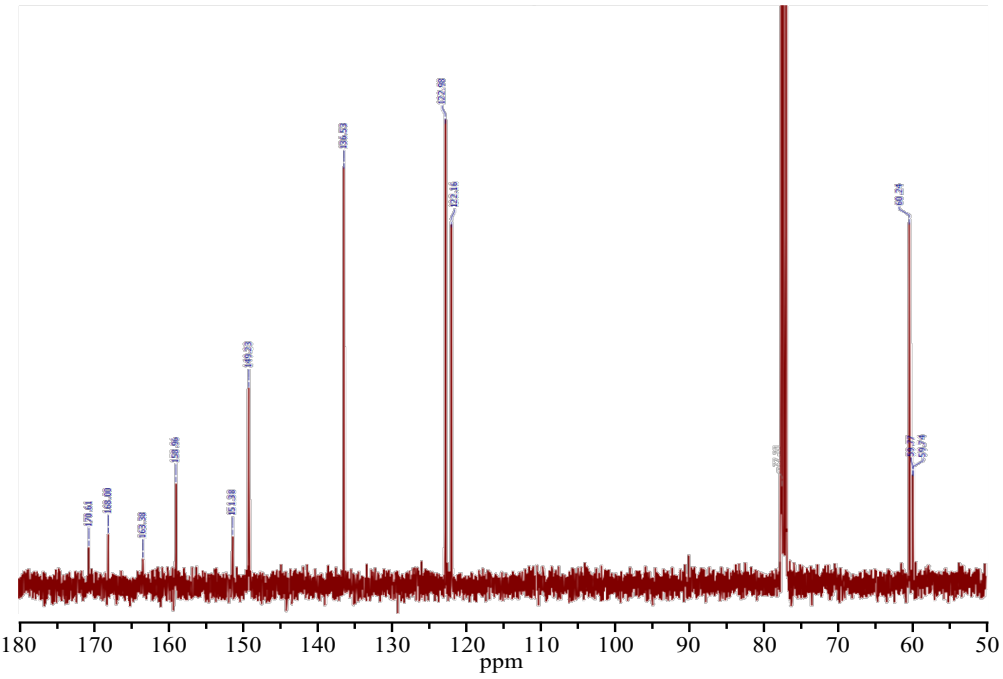

Figure 5. ^{13}C NMR spectrum of ^{19}F-TPA (100 MHz, $CDCl_3$) δ 170.61, 168.00, 163.38, 158.96, 151.38, 149.23, 136.53, 122.98, 122.16, 60.24, 59.77, 59.74.

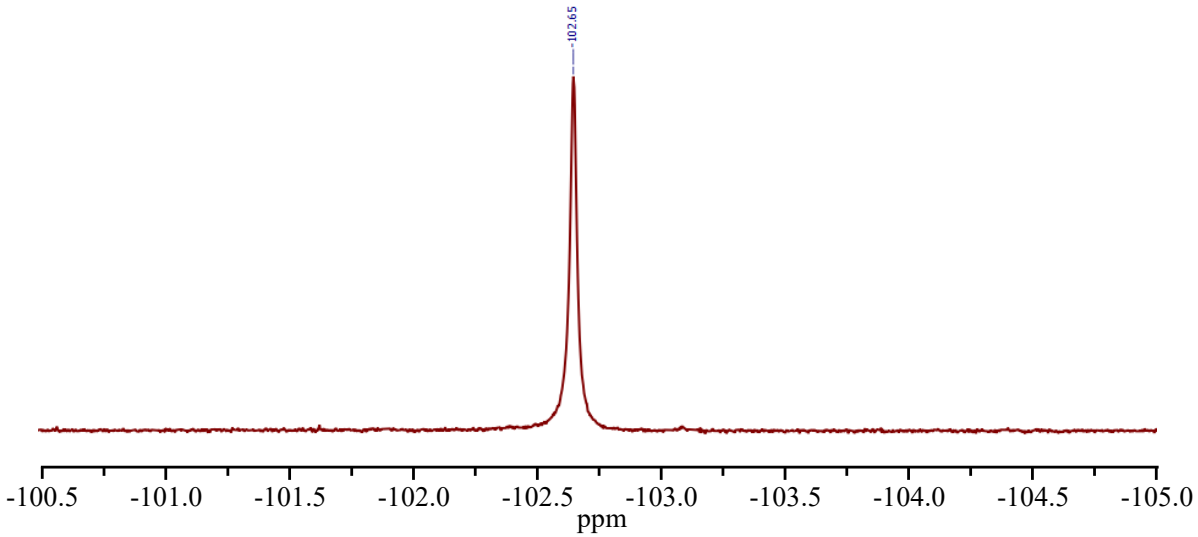

Figure 6. ^{19}F NMR spectrum of ^{19}F-TPA (400 MHz, $CDCl_3$) δ -102.56.

Analytical HPLC was used to characterize the Zn binding properties of ^{18}F-TPA to identify the Zn free ^{18}F-TPA ligand and Zn bound ^{18}F-TPA complex. In achieving this, HPLC characterization was done by continuously adding Zn^{+2} into ^{19}F-TPA and tracking the changes of the peaks as evidence of formation of the Zn^{19}F-TPA complex. **Figure 7A-C** indicate that ^{19}F-TPA was prone to bind with Zn quickly. Importantly, the

two compounds, when Zn is added, can be detected by HPLC suggesting the feasibility of in vitro ^{18}F-TPA studies.

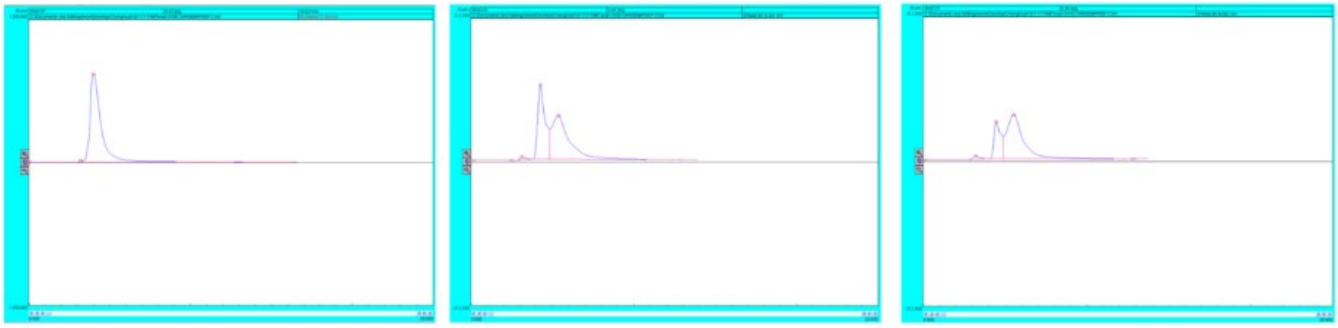

Figure 7. Analytical HPLC chromatograms of ^{19}F-TPA and Zn^{19}F-TPA with the following conditions: Luna 5 µm C18(2) reserved phase column, mobile phase of CH_3CN: H_2O of 40:60, wavelength of 254 nm and flow rate of 1 mL/min. (A) ^{19}F-TPA with no Zn^{+2}, (B) addition of Zn^{+2} to ^{19}F-TPA, (C) higher levels of Zn^{+2} to ^{19}F-TPA.

Characterization of NO_2-TPA

In optimizing the semiprep HPLC conditions to isolate ^{18}F-TPA from its precursor, a mixture of NO_2-TPA and ^{19}F-TPA was used with ^{19}F-TPA acting in place of ^{18}F-TPA. **Figure 8** demonstrates only ^{19}F-TPA using a semiprep CH_3CN: H_2O = 40:60 solvent condition with a Luna 10 µm C18(2) reversed phase column at a wavelength of 254 nm and flow rate of 5 mL/min. This provided the retention time, 7.98 minutes, which was then used to identify the signal of ^{19}F-TPA in the subsequent HPLC data obtained from the mixture of NO_2-TPA and ^{19}F-TPA. **Figure 9** depicts sufficient separation of ^{19}F-TPA and NO_2-TPA with a CH_3CN: H_2O = 40:60 solvent condition resulting in retention times at 7.36 and 9.33 minutes, respectively. The same semi-prep HPLC conditions used to determine the retention time for ^{19}F-TPA were used for determining the separation of ^{19}F-TPA and NO_2-TPA.

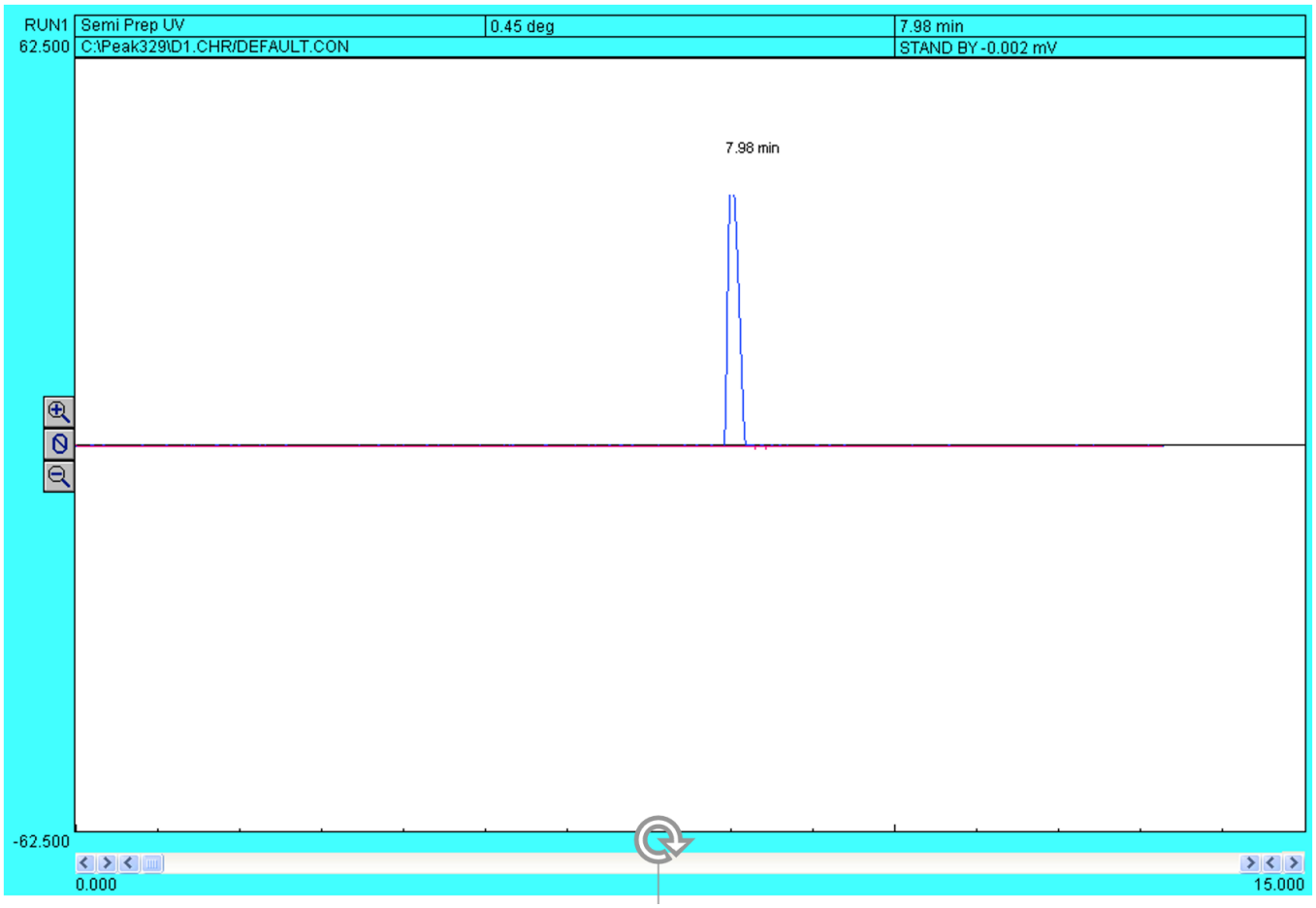

Figure 8. Semiprep HPLC chromatogram of ^{19}F-TPA with retention time of 7.98 minutes using CH_3CN:H_2O = 40:60 solvent condition, Luna 10 µm C18(2) reversed phase column, wavelength of 254 nm, and flow rate of 5 mL/min.

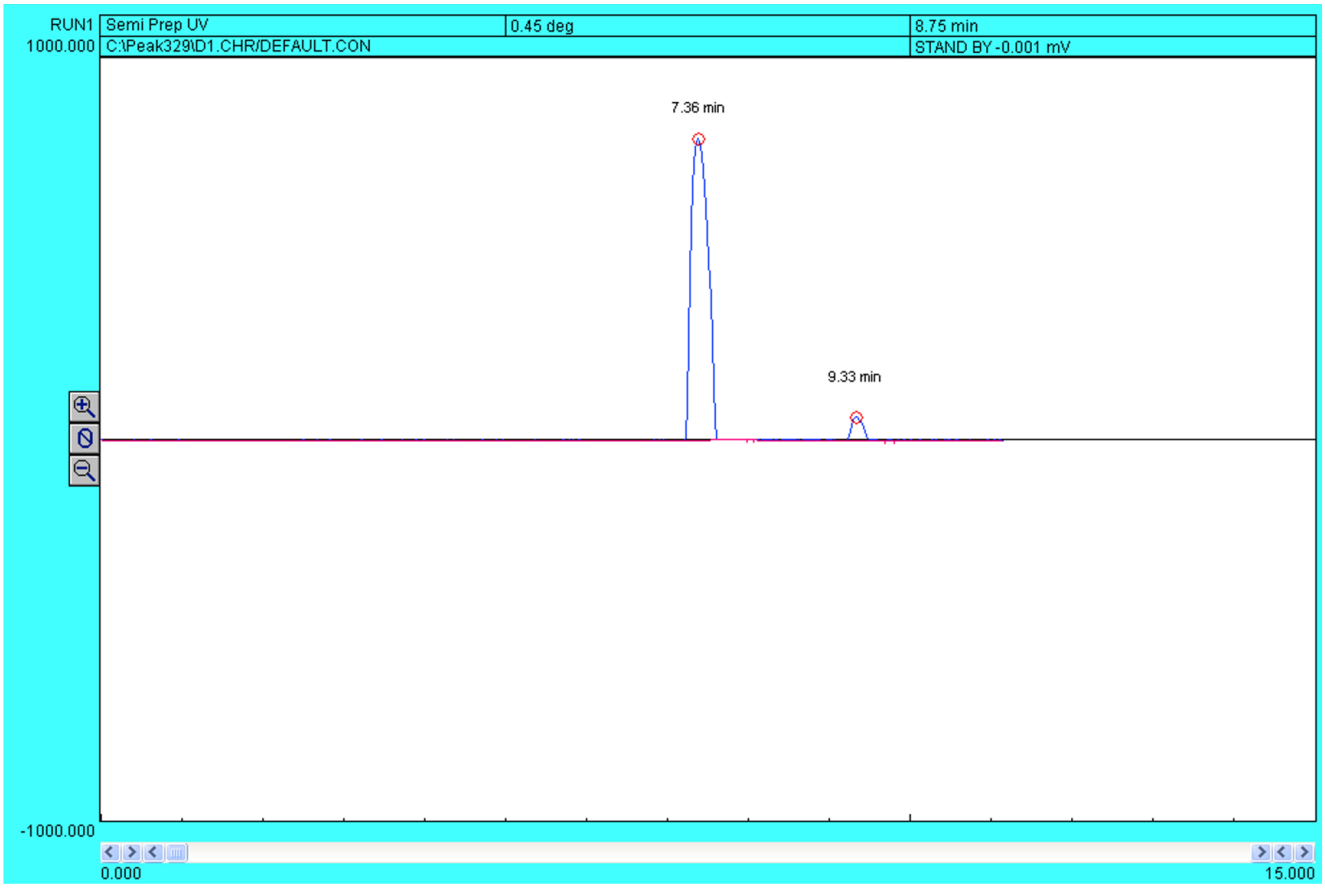

Figure 9. Semi-prep HPLC chromatogram of mixture of NO_2-TPA and ^{19}F-TPA. First retention time is ^{19}F-TPA at 7.36 min. Second retention time is NO_2-TPA at 9.33 min. HPLC conditions are the following: CH_3CN:H_2O = 40:60 solvent condition, Luna 10 µm C18(2) reversed phase column, wavelength of 254 nm, and flow rate of 5 mL/min.

Characterization of ^{18}F-TPA

The ^{18}F-TPA compound was prepared (**Figure 3B**) and purified using the determined condition found above, of CH_3CN: H_2O = 40:60 from semiprep HPLC. Its characterization relied on the same retention time in the radiation (Rad) channel with that of ^{19}F-TPA in the UV channel. The ^{18}F-TPA compound retention time was determined first using analytical HPLC. **Figure 10** depicts the purified ^{18}F-TPA compound in the Rad channel with the use of a Luna 5 µm C18(2) reversed phase column, CH_3CN: H_2O = 40:60 solvent condition, wavelength of 254 nm and flow rate of 1 mL/min. Co-injection of ^{19}F-TPA (**Figure 11A**) and ^{18}F-TPA (**Figure 11B**) was done to verify the synthesis of the probe using the same analytical HPLC conditions to obtain ^{18}F-TPA HPLC chromatogram. **Figure 11** demonstrates the successful preparation and purification of ^{18}F-TPA as

evidence by the similar retention times of the two compounds. This procedure for ^{18}F-TPA, discussed in the methods section, was used for the preparation of ^{18}F-TPA for subsequent *in vitro* and *in vivo* studies.

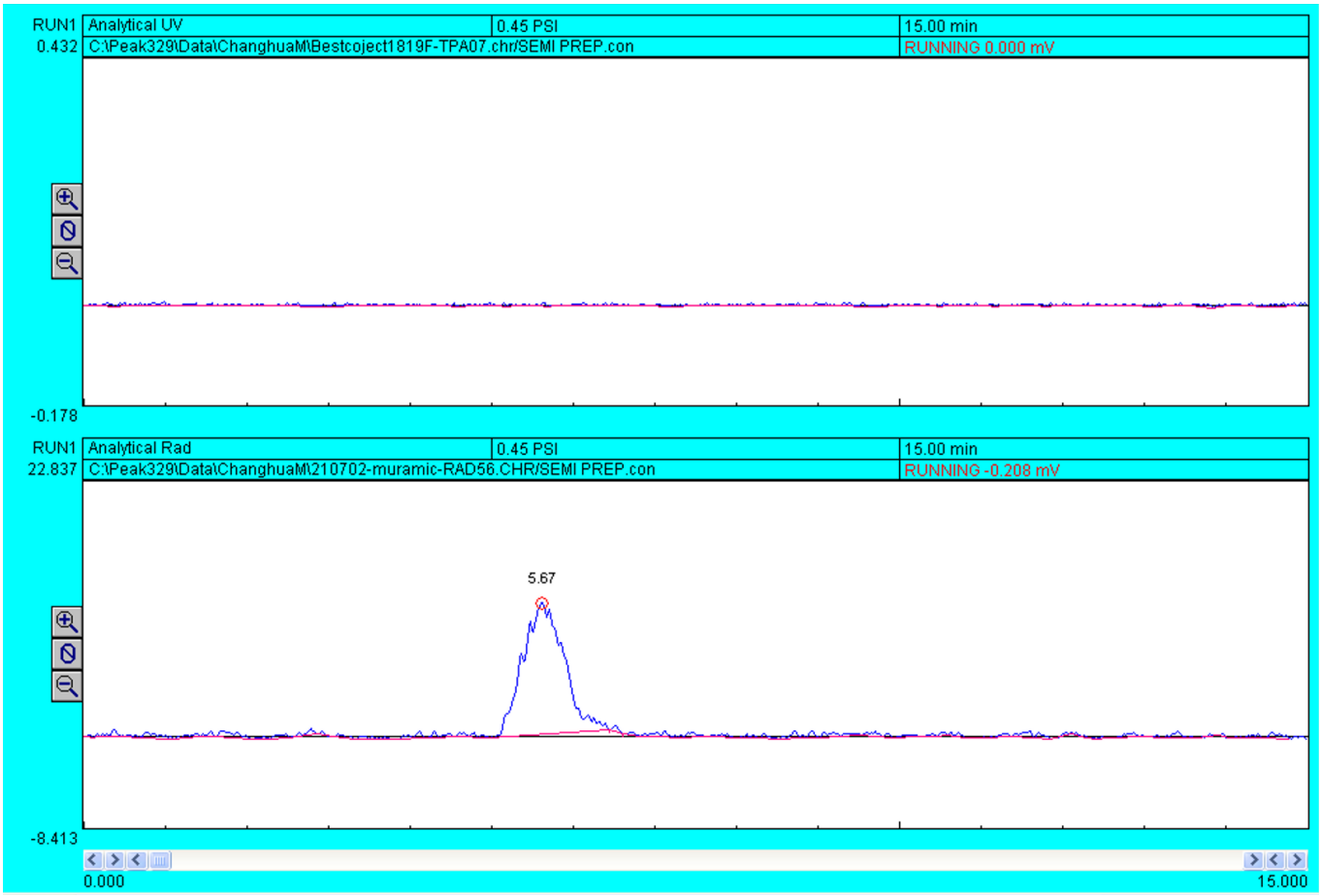

Figure 10: Analytical HPLC of purified ^{18}F-TPA at 5.67 minutes retention time using the following conditions: Luna 5 µm C18(2) reversed phase column, CH_3CN:H_2O = 40:60 solvent condition, 254 nm wavelength, 1mL/min flow rate.

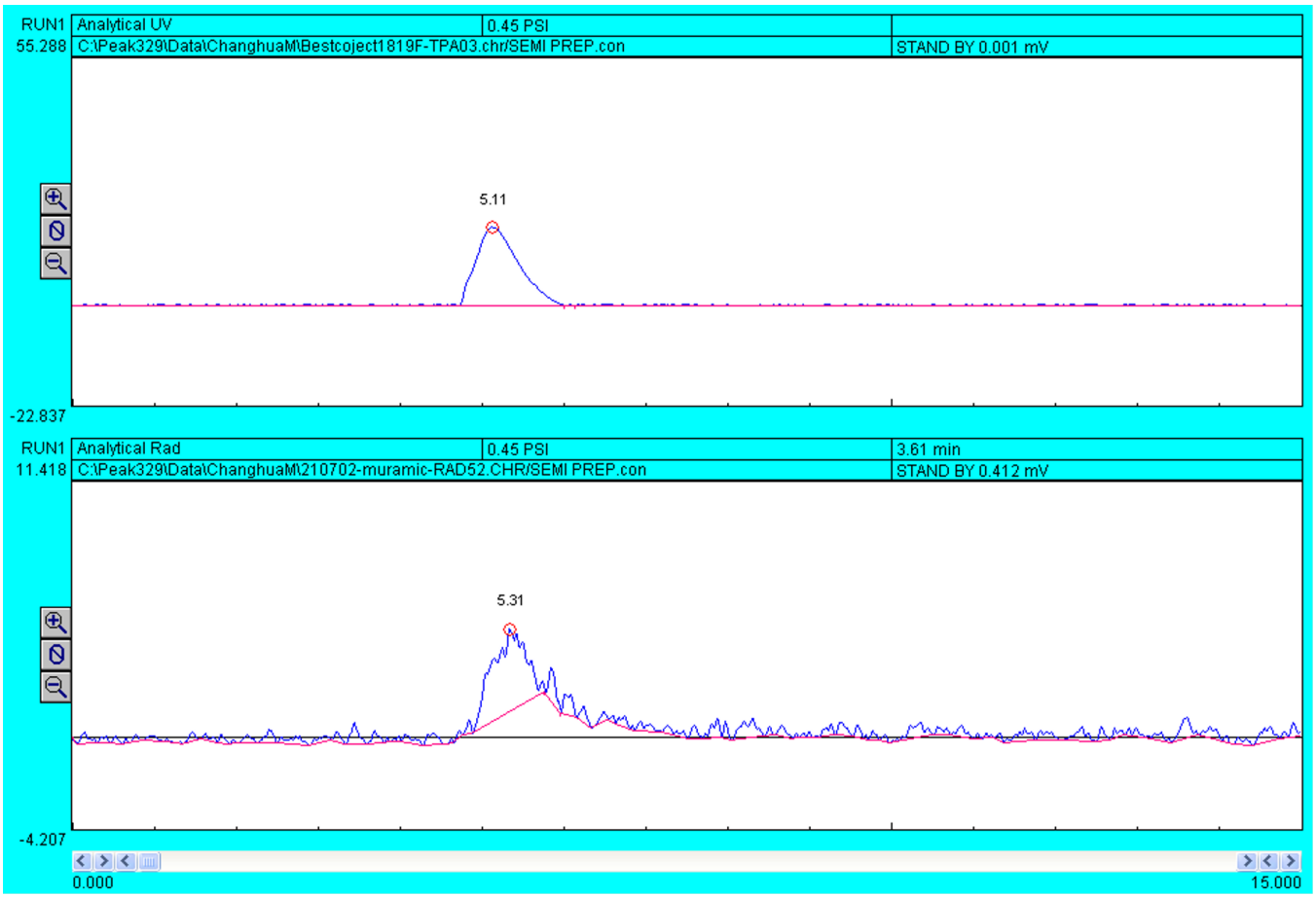

Figure 11: Analytical HPLC of co-injection of ^{18}F-TPA and ^{19}F-TPA using the following conditions: C18 reserve column, $CH_3CN:H_2O$ = 40:60 solvent condition, 254 nm wavelength, 1mL/min flow rate. (A) In the UV channel, ^{19}F-TPA has a retention time of 5.11 minutes. (B) In the Rad channel, ^{18}F-TPA has a retention time of 5.31 minutes.

Characterization of ^{18}F-TPA zinc probe with *in vitro* assays

A cell binding assay was done to demonstrate the intracellular Zinc detection by the developed ^{18}F-TPA with radioactivity reported in CPM using a Hidex gamma counter (**Figure 12**). The ^{18}F conjugated TPA ligands were administered to the 22Rv1 cells in serum free media with or without pre-treatment of cold TPA and a known Zn^{2+} chelator (TPEN) and were incubated for 1.5 hours. It was observed that the ^{18}F-TPA was significantly retained within the cells in the absence of the blocking agents. However, approximately 75% of the ^{18}F-TPA cell associated activity was reduced in the presence of 1 μM of the blocking agents. It was found that TPEN was more efficient with intracellular Zn^{2+} chelation to that of the cold TPA.

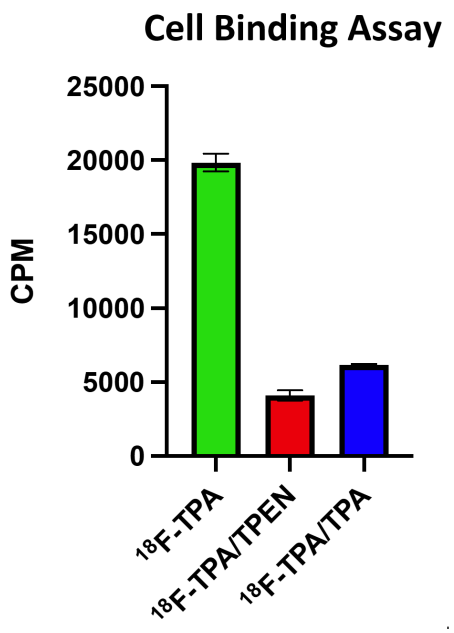

Figure 12. Bar graph of intracellular Zn^{2+} cell binding assay in 22rv1 cells with radioactivity reported in CPM. From left to right: ^{18}F-TPA probe uptake group, standard Zn^{2+} chelator TPEN (1 μM) as the blocking agent followed by ^{18}F-TPA probe introduction, and Zn^{2+} chelator TPA (1 μM) ligand as blocking agent followed by ^{18}F-TPA probe introduction.

Discussion

The goal of this project was to develop a novel PET imaging method for the detection of aggressive PCa through achieving three stages of research: (i) synthesis and characterization of Zn^{+2} targeting ^{18}F-TPA radionuclide and its model version ^{19}F-TPA, (ii) evaluation of ^{18}F-TPA probe's Zn binding capabilities in *in vitro* assays, (iii) PET imaging studies of Zn distribution *in vivo* using ^{18}F-TPA probe.

The study started with the successful optimization, from previously reported methods, and synthesis of ^{19}F-TPA. The ^{1}H (**Figure 4**), ^{13}C (**Figure 5**), and ^{19}F (**Figure 6**)NMR data demonstrate ^{19}F-TPA was synthesized with high yield and purity. ^{19}F-TPA was used as a reference compound of ^{18}F-TPA to identify HPLC conditions for purification of ^{18}F-TPA from the reaction mixture, verification of ^{18}F-TPA synthesis, and evaluation of the probe's binding capability to Zn.

The HPLC data obtained (**Figure 7**) demonstrates Zn^{19}F-TPA complex formation. When additional Zn is added into a sample of ^{19}F-TPA, ^{19}F-TPA molecules get converted to Zn^{19}F-TPA complexes. The data provides strong evidence to prove the concept that Zn binding takes place. However, additional studies will need to be

done to determine if Zn binding is a 1:1 ratio and how much Zn is necessary among other details. These details will be determined by a thorough study to further characterize this binding.

The probe's synthesis was the critical step for this study. Previously reported methods were applied to prepare ^{18}F labelled pyridyl compounds using nitro-pyridyl compound as the precursor. The synthesis started with preparing 2-(bromomethyl)-4-nitropyridine then further reacting it with di-(2-picolyl)amine under similar conditions of synthesizing ^{19}F-TPA to produce NO_2-TPA. The substitution reaction of NO_2-TPA to ^{18}F-TPA resulted in high yield (~50%) and in a short amount of time (15 minutes) providing a great method for preparing ^{18}F-label compounds.

The HPLC data (**Figure 10 and 11**) provides strong evidence of the successful synthesis of ^{18}F-TPA. **Figure 10** demonstrates no signals on the UV channel signifying the purity of the ^{18}F-TPA compound. **Figure 11** demonstrates the co-injection of ^{19}F-TPA and ^{18}F-TPA have the same retention time verifying the synthesis was successful. The high yield reaction, optimized semi-prep HPLC conditions, and optimized fast processing procedure provided a consistently high intensity of pure ^{18}F-TPA by the end of the synthesis. An isolation of ~37 MBq (~1 mCi) of pure ^{18}F-TPA had been successfully utilized in the subsequent cell binding assay.

A cell binding assay was done with the goal to prove the trapping mechanism of ^{18}F-TPA as it binds to intracellular Zn^{2+} and demonstrates Zn^{2+} specificity. The preliminary data obtained from the in vitro cell binding assay provides promising results however further testing will need to be done to strongly support the hypothesis that ^{18}F-TPA can selectively bind to the intracellular Zn^{2+} (**Figure 12**). The high uptake of ^{18}F-TPA in the absent of any blocking agent, compared to those with the blocking agents, suggest that the developed probe possibly can chelate to intracellular Zn^{2+} and the Zn complex of ^{18}F-TPA can be trapped within the cell. This high uptake seen with this cell line will need to be compared to healthy cells to determine if internationalization is present. Intracellular Zn^{2+} was chelated by treatment of a known Zn^{2+} chelator (TPEN) or TPA which may have reduced the uptake of ^{18}F-TPA. Furthermore, by comparing the blocking efficacy of TPEN and TPA, it could be concluded that TPEN is a highly potent chelator of Zn^{2+}, aligning with previously reported studies.

There remains the possibility that the probe could be membrane bound thus supporting the high CPM

levels. The membrane wasn't separated from the internal components from the cell therefore the data is not sufficient to provide a conclusory statement that the hypothesis is correct. This limitation will be addressed with the inclusion of an extra step to remove the cell membrane from the rest of the cell. Another possibility that can be interpreted from this result is the binding affinity may have been affected. It was expected that with PCa cell lines, there should be significantly low readout due to the low levels of intracellular Zn^{2+}. The high readout from this PCa cell line can indicate non-specific binding. The electron-withdrawing fluorine atom, at the para-position of the pyridine in the ^{18}F-TPA molecule, weakens the binding affinity of the probe with Zn^{2+} resulting in a non-specific binding with other ions in the cell. Without results from a positive control of healthy cells, it is difficult to make any conclusive statements that the probe has been successfully internalized and trapped within the cell. A thorough analysis will be needed for future cell binding assays as well as repeating this experiment to validate the feasibility of the probe.

The results obtained thus far with the Zn binding properties of the probe and its possibility of internalization in the cell have provided further exploration into the hypothesis regarding the probe's behavior. The TPA compound itself has Zn specificity and its cell permeability characteristic previously proven have demonstrated similar conclusion through the data obtained from this study. This justifies the direction this project is heading towards.

Future Work

Characterization of ^{18}F-TPA with in vitro assays

Current analysis in determining Zn concentration and performing the statistical analysis is still in progress for the 22rv1 cells that were used for the cell binding assay. Future studies would examine the probe's behavior in zinc rich cell line, R7T1, zinc poor cell line, HEK-293T, and other PCa cell lines such as PC3. The R7T1 cell line will represent a healthy cell while the HEK-293T cell line will represent a diseased state. Other PCa cell lines are being tested to provide more information as to how this probe behaves and if consistent results can be seen as with the cell binding assay done for the 22rv1 PCa cell line. All these cell lines will be used to perform the same cell binding assay as previously described in the methods section. What would be added to this procedure will be a consideration of separating the membrane from the internal components of the cell.

The R7T1 cells would demonstrate high uptake of the probe, as represented by CPM, for all three groups. It is expected that a 10-fold difference will be seen with the uptake group (only the probe) in comparison to the uptake group with the 22rv1 cell line. This is due to previous studies that have reported R7T1 as a cell with high levels of zinc of 380 nmol zinc/g protein.[23] This can be compared to HEK-293T cell zinc content which is reported to be 34 nmol zinc/g protein.[23] The HEK-293T and other PCa cell lines that will be used will demonstrate low CPM levels, similar to what was obtained for the 22rv1 cell line. It is expected that regardless of the type of cell line used, the blocking groups will demonstrate low CPM levels compared to the uptake group.

Thorough work would need to be done to optimize the conditions of the in vitro protocols to provide overall accurate assessment of the probe's behavior. Additional work such as a saturation assay in determining how much probe should be introduced into the cell and time related assay to determine how long the probe and blocking agents should be incubated for. With the probe characterized with these studies, in vivo testing can be performed.

µPET/CT Imaging Study

Currently, the PET images have been acquired however biodistribution analysis and PET analysis is currently in progress and thus will not be reported in this report.

Image Processing and Analysis

AMIDE, a multimodal medical imaging processing software, will be used to view, process, and analyze the images. The register image provided the transverse, coronal, and sagittal views, all used to draw region of interests (ROIs). In vivo ROIs, using the free hand shape, will be used to outline areas of Zn uptake for the areas of radioactivity decay. Numerical data will be extracted from these images for further analysis. The maximum standard uptake volume (SUVmax) and percent injected dose per gram (%i.d./g) will be calculated, and time activity curves (TACs) will be generated.

Expected Results and Discussion

The animal study is estimated to demonstrate that ^{18}F-TPA would have high uptake in Zn rich tissues such as the prostate for healthy mice. Subsequent studies would be done on prostate cancer mice models using

the same protocol as described in the methods. The probe uptake would be quantified by calculating SUVmax and %Id/g. SUVmax is a widely used robust quantifier calculated by calculating the SUV on the highest image pixel in the drawn ROIs for each organ. Despite it being commonly used in the quantification of probe uptake and providing lower inter-observer variability, it can be affected by image reconstruction parameters such as point-spread-function providing higher SUVmax values.[24] Additionally, it can be amenable to confounding variables such as scanner resolution, body characteristics, and tracer pharmacokinetics.[25]

These limitations would be taken into consideration while making the conclusions necessary to support the hypothesis. The %id/g would also be calculated which would be helpful in providing a semi-quantitative and reliable estimate of probe uptake. Due to high probe uptake, it is anticipated that %id/g and SUVmax values would be higher in healthy mice models than in PCa mice models.

One of the major challenges in this study is the images resulting from probe uptake in PCa mouse models. Due to the biological process of PCa, where Zn concentrations are significantly decreased, it is expected that probe uptake would be significantly low in the PCa mice in comparison to the healthy mice models. Hence, probe uptake would be minimal with high background noise with the PCa mice due to the presence of Zn in all the organs. This will be mitigated through optimizing the protocol.

The biodistribution studies are expected to have high probe uptake in the organs of the healthy mice versus the PCa mice and these results should be in line to the image analysis and probe quantification. Additionally, the organs would be harvested, and Zn concentrations would be quantified to support the expected high/low probe uptake.

Conclusion

The preliminary data demonstrates that the synthesis portion of the project has been successful. The data obtained from the HPLC for each step of the chemical synthesis for the standard reference and probe have demonstrated that the process has been done correctly. The *in vitro* cell binding assay performed thus far has provided results that supports further evaluation and testing to characterize the cell internalization of the probe as it binds to Zn. The work on the *in vitro* assays and animal studies are progressing.

Future work will be done on additional *in vitro* assays to provide further evidence of its trapping behavior and

specificity, and the use of prostate cancer mice models to examine the behavior of the probe. The project's results thus far have been encouraging in the potential of the effectiveness the ^{18}F-TPA probe provides to visualize zinc distribution with the goal of transitioning to clinical trials with the application of monitoring PCa.

References

[1] Gis.cdc.gov. 2021. USCS Data Visualizations. [online] Available at: <https://gis.cdc.gov/Cancer/USCS/DataViz.html> [Accessed 30 May 2021].

[2] Yuan Y, Wei Z, Chu C, et al. Development of Zinc-Specific iCEST MRI as an Imaging Biomarker for Prostate Cancer. Angew Chem Int Ed Engl. 2019;58(43):15512-15517. doi:10.1002/anie.201909429

[3] Lo ST, Martins AF, Jordan VC, Sherry AD. Zinc as an Imaging Biomarker of Prostate Cancer. Isr J Chem. 2017;57(9):854-861. doi:10.1002/ijch.201700043

[4] Turkbey B, Choyke PL. Future Perspectives and Challenges of Prostate MR Imaging. Radiol Clin North Am. 2018;56(2):327-337. doi:10.1016/j.rcl.2017.10.013

[5] Maret, W. in Interrelations between Essential Metal Ions and Human Diseases (eds Astrid Sigel, Helmut Sigel, & Roland K. O. Sigel) 389-414 (Springer Netherlands, 2013).

[6] Rana, U. et al. Zinc binding ligands and cellular zinc trafficking: Apo-metallothionein, glutathione, TPEN, proteomic zinc, and Zn-Sp1. Journal of Inorganic Biochemistry 102, 489-499, doi:https://doi.org/10.1016/j.jinorgbio.2007.10.030 (2008).

[7] Maret, W. Zinc in pancreatic islet biology, insulin sensitivity, and diabetes. Preventive nutrition and food science 22, 1 (2017).

[8] Maret, W. Analyzing free zinc(II) ion concentrations in cell biology with fluorescent chelating molecules. Metallomics 7, 202-211, doi:10.1039/c4mt00230j (2015).

[9] Chimienti, F. et al. In vivo expression and functional characterization of the zinc transporter ZnT8 in glucose-induced insulin secretion. Journal of Cell Science 119, 4199-4206, doi:10.1242/jcs.03164 (2006).

[10] Franz MC, Anderle P, Bürzle M, et al. Zinc transporters in prostate cancer. Mol Aspects Med. 2013;34(2-3):735-741. doi:10.1016/j.mam.2012.11.007

[11] Costello LC, Franklin RB. A comprehensive review of the role of zinc in normal prostate function and metabolism; and its implications in prostate cancer. Arch Biochem Biophys. 2016;611:100-112. doi:10.1016/j.abb.2016.04.014

[12] Costello, L. C. & Franklin, R. B. Cytotoxic/tumor suppressor role of zinc for the treatment of cancer: an

enigma and an opportunity. Expert review of anticancer therapy 12, 121-128, doi:10.1586/era.11.190 (2012).

[13] Li D, Stovall DB, Wang W, Sui G. Advances of Zinc Signaling Studies in Prostate Cancer. Int J Mol Sci. 2020;21(2):667. Published 2020 Jan 19. doi:10.3390/ijms21020667

[14] Ghosh SK, Kim P, Zhang XA, et al. A novel imaging approach for early detection of prostate cancer based on endogenous zinc sensing. Cancer Res. 2010;70(15):6119-6127. doi:10.1158/0008-5472.CAN-10-1008

[15] Clavijo Jordan MV, Lo ST, Chen S, et al. Zinc-sensitive MRI contrast agent detects differential release of Zn(II) ions from the healthy vs. malignant mouse prostate. Proc Natl Acad Sci U S A. 2016;113(37):E5464-E5471. doi:10.1073/pnas.1609450113

[16] Sai KKS, Zachar Z, Bingham PM, Mintz A. Metabolic PET Imaging in Oncology. AJR Am J Roentgenol. 2017;209(2):270-276. doi:10.2214/AJR.17.18112

[17] Liang, S. H. et al. PET Neuroimaging Studies of [18F]CABS13 in a Double Transgenic Mouse Model of Alzheimer's Disease and Nonhuman Primates. ACS Chemical Neuroscience 6, 535-541, doi:10.1021/acschemneuro.5b00055 (2015).

[18] Cary, B. P. et al. Targeting Metal-Aβ Aggregates with Bifunctional Radioligand [11C]L2-b and a Fluorine-18 Analogue [18F]FL2-b. ACS Medicinal Chemistry Letters 6, 112-116, doi:10.1021/ml500413d (2015).

[19] Huang Z, Zhang XA, Bosch M, Smith SJ, Lippard SJ. Tris(2-pyridylmethyl)amine (TPA) as a membrane-permeable chelator for interception of biological mobile zinc. Metallomics. 2013;5(6):648-655. doi:10.1039/c3mt00103b

[20] Shen, B., et al., Nucleophilic [18F]fluorination and subsequent decarbonylation of methoxy-substituted nitroand halogen-benzenes activated by one or two formyl groups. J. Labelled Compd. Radiopharm., 2010. 53: p. 113-119.

[21] Jacobson, O., D.O. Kiesewetter, and X. Chen, Fluorine-18 Radiochemistry, Labeling Strategies and Synthetic Routes. Bioconjugate Chem., 2015. 26: p. 1-18.

[22] Yan, M., Song, Y., Wong, C. P., Hardin, K. & Ho, E. Zinc deficiency alters DNA damage response genes in normal human prostate epithelial cells. J Nutr 138, 667-673, doi:10.1093/jn/138.4.667 (2008).

[23] Hyun, H. J. et al. Depletion of Intracellular Zinc and Copper with TPEN Results in Apoptosis of Cultured

Human Retinal Pigment Epithelial Cells. Investigative Ophthalmology & Visual Science 42, 460-465 (2001).

[24] Rogasch JM, Steffen IG, Hofheinz F, et al. The association of tumor-to-background ratios and SUVmax deviations related to point spread function and time-of-flight F18-FDG-PET/CT reconstruction in colorectal liver metastases. EJNMMI Res. 2015;5:31. Published 2015 May 6. doi:10.1186/s13550-015-0111-5

[25] Gross L, Paintmayer L, Lehner S, et al. FDG-PET reveals improved cardiac regeneration and attenuated adverse remodelling following Sitagliptin + G-CSF therapy after acute myocardial infarction. Eur Heart J Cardiovasc Imaging. 2016;17(2):136-145. doi:10.1093/ehjci/jev237

Publishing Agreement

It is the policy of the University to encourage open access and broad distribution of all theses, dissertations, and manuscripts. The Graduate Division will facilitate the distribution of UCSF theses, dissertations, and manuscripts to the UCSF Library for open access and distribution. UCSF will make such theses, dissertations, and manuscripts accessible to the public and will take reasonable steps to preserve these works in perpetuity.

I hereby grant the non-exclusive, perpetual right to The Regents of the University of California to reproduce, publicly display, distribute, preserve, and publish copies of my thesis, dissertation, or manuscript in any form or media, now existing or later derived, including access online for teaching, research, and public service purposes.

DocuSigned by:
Umama Ali
366173AB43954D9...
Author Signature

8/30/2021
Date